AIAA JOURNAL
Vol. 44, No. 10, October 2006

Parameter Optimization of the Dynamic Behavior of Inhomogeneous Multifunctional Power Structures

C. W. Schwingshackl*
Imperial College London, London, SW7 2AZ England, United Kingdom
G. S. Aglietti†
University of Southampton, Southampton, SO17 1BJ England, United Kingdom
and
P. R. Cunningham‡
Smiths Aerospace Mechanical Systems–Aerostructures, Hamble-le-Rice, SO31 4NF England, United Kingdom

DOI: 10.2514/1.18599

For next generation microsatellites and nanosatellites, new design approaches will be required to significantly increase their payload to mass fraction. One proposed technology is the multifunctional design concept that incorporates spacecraft subsystems into the load carrying structure. The focus of the research is the multifunctional power structure which replaces conventional battery systems in a spacecraft. An analytical and finite element analysis of ten multifunctional sandwich structures is presented. The out-of-plane material properties are discussed and a parameter optimization of the ten sandwich panels is carried out to optimize their frequency to density ratio. The best configuration for an optimized multifunctional power structure is then identified from the analytical and finite element investigation. The optimized design provides a similar predicted dynamic response as a conventional honeycomb sandwich panel, and can be considered a serious alternative for future spacecraft.

Nomenclature

a	=	length
b	=	width
E	=	Young's modulus
F	=	force
G	=	shear modulus
H	=	horizontal reaction force
h	=	height
J	=	second area moment of inertia
l	=	corrugation leg length
M	=	reaction moments
N	=	normal forces
n	=	number of
s	=	path
t	=	thickness
U	=	potential energy
V	=	vertical reaction force
ν	=	Poisson ratio
ρ	=	density
τ	=	shear stress
φ	=	corrugation angle
ω	=	frequency

Subscripts

AA, BB, CC	=	joints
B	=	bicell
C	=	core
CORR	=	corrugation
CV	=	control volume
I, II	=	corrugation leg 1 and 2
F	=	face skins
mat	=	material
P	=	panel
pow	=	power
xz, yz	=	x–z, y–z-plane

Received 6 July 2005; accepted for publication 7 July 2006.

*Research Associate, Center of Vibration Engineering, Mechanical Engineering, Exhibition Road, London.
†Senior Lecturer in Aerospace Structural Dynamics, Astronautics Research Group, School of Engineering Sciences, Highfield, Southampton.
‡Principal Stress Engineer, SAMS-A, Kings Avenue, Hamble-le-Rice, Southampton.

I. Introduction

A common goal of spacecraft engineering is the design and fabrication of lighter, smaller, and cheaper satellites. To achieve these aims in the near future, space agencies are considering the launch and operation of large numbers of miniature spacecraft with an order of magnitude reduction in flight mass from today's spacecraft for next generation microsatellites (100-10 kg) and nanosatellites (<10 kg) [1,2]. In the course of this development, recent advances in technology must be applied to provide extended capabilities of the spacecraft in terms of lower mass and volume.

The multifunctional structure (MFS) is a feasible new approach for future spacecraft requirements. It merges the load carrying capabilities of traditional spacecraft structures with other stand-alone functions leading to a significant mass and volume reduction. Secondary subsystems such as microelectronics, microinstrumentation, sensors, data handling, flexible circuitry, power generation and storage, thermal management, radiation shielding, and propulsion [3] are items that are considered for integration in a MFS. Currently, these subsystems are manufactured and packaged separately, adding heavy containers, load bearing plates and frames, bulky wire harnesses, and connectors to the final assembly of the spacecraft. Guerrero et al. [4] estimate that a fully applied multifunctional approach could reduce the volume and mass of a spacecraft by up to 80% and 90%, respectively, and decrease assembly and rework labor by up to 50%.

Power storage systems are considered a key to cost-effective space missions and therefore a primary target for multifunctional applications. Traditional stand-alone energy storage systems, consisting of separated cells in bulky containers, account for about 20–30% of the total satellite mass and occupy a significant portion of

the spacecraft volume [5]. A MFS approach could drastically reduce the mass and volume of an onboard power storage system. The lithium battery in a honeycomb core technology developed by ITN Energy Systems, uses thin-film solid-state lithium batteries attached to the available surface area of a conventional honeycomb core [6,7]. A variation of this technology implements several thin battery layers as the structural face sheets of a sandwich panel. A further approach to the MFS power concept by ITN are solid-state thin-film rechargeable batteries on fiber substrate (PowerFibers) that can be utilized as individual reinforcement fibers in composite materials [8]. Other developments include those by Boundless Corp. who have reconfigured the battery material as a structural support for the spacecraft [9–11]. Ribbonlike positive and negative electrodes are laminated into a monolithic electrode stack and used as bulky core materials for a sandwich panel.

Any investigation into possible multifunctional power structures must consider the electrochemical and structural behavior. The electrochemical aspects have so far been the main focus in the literature and the structural and dynamic area has not been investigated in any detail. The research presented herein supplements the structural and dynamic analysis of possible multifunctional power structures. The equivalent material properties of ten MFS designs are derived and a parameter optimization of the dynamic aspects is presented to provide high stiffness and low mass at an adequate electric power density. Comparisons with a conventional honeycomb core sandwich panel in terms of structural performance are provided and a final optimized MFS approach is discussed.

II. Multifunctional Power Structure

The requirements for a multifunctional power storage structure are manifold. It has to integrate the batteries into the structure, provide the requested electrical properties, show a satisfying structural and dynamic behavior, and be a lightweight and reliable technology for use in space. In addition, it needs to remain user-friendly to the rest of the spacecraft, must not hinder the use of the satellite, and has to provide servicing functions during integration and testing [2].

The investigation of the multifunctional power structure implemented the structural batteries (bicells) presented by Boundless Corp. [9,10,12]. An estimated dimension of $0.14 \times 0.02 \times 0.0015$ m was assumed for the flat and sinusoidal batteries. Their design provides multifunctionality at the electrode level making them a primary structural element in a multifunctional sandwich panel. This approach leads to two possible configurations of a multifunctional power structure: the bicells entirely replace the conventional core materials in the sandwich and provide all the structural support, or the bicells are embedded into conventional core materials, such as honeycomb or corrugated core which adds additional stiffness to the structure and reduces the usually orthotropic behavior of the core. In the first case, the demands for the bicells are particularly high as no additional supporting core structure is available. In the latter case, the structural requirements for the bicell are lower but additional issues such as the assembly and interaction of the different components could arise.

Ten possible candidate designs have been considered as a multifunctional power structure including a bicell–honeycomb combination, pure bicell cores, and a variety of bicell–corrugation combinations (see Fig. 1).

III. Simplified Material Properties of Different MFS Designs

The dynamic behavior during launch and flight is a very important design aspect for space qualified sandwich structures. A wide range of theoretical models of the dynamic response of orthotropic sandwich plates is available [13–17] and in this particular research Ravill's [17] approach, which has been validated by Narayana [18], will be used. This theory for a simply supported sandwich panel (see Fig. 2) of core length a_C, core width b_C, and core height h_C, incorporates an orthotropic core with the corresponding out-of-plane shear moduli $G_{C_{xz}}$ and $G_{C_{yz}}$. It assumes an infinite out-of-plane Young's modulus E_{C_z} of the core, and regards the shear stresses τ_{xz}, τ_{yz} to be independent of z. Based on these assumptions, an equation for the flexural vibration of a simply supported sandwich panels is

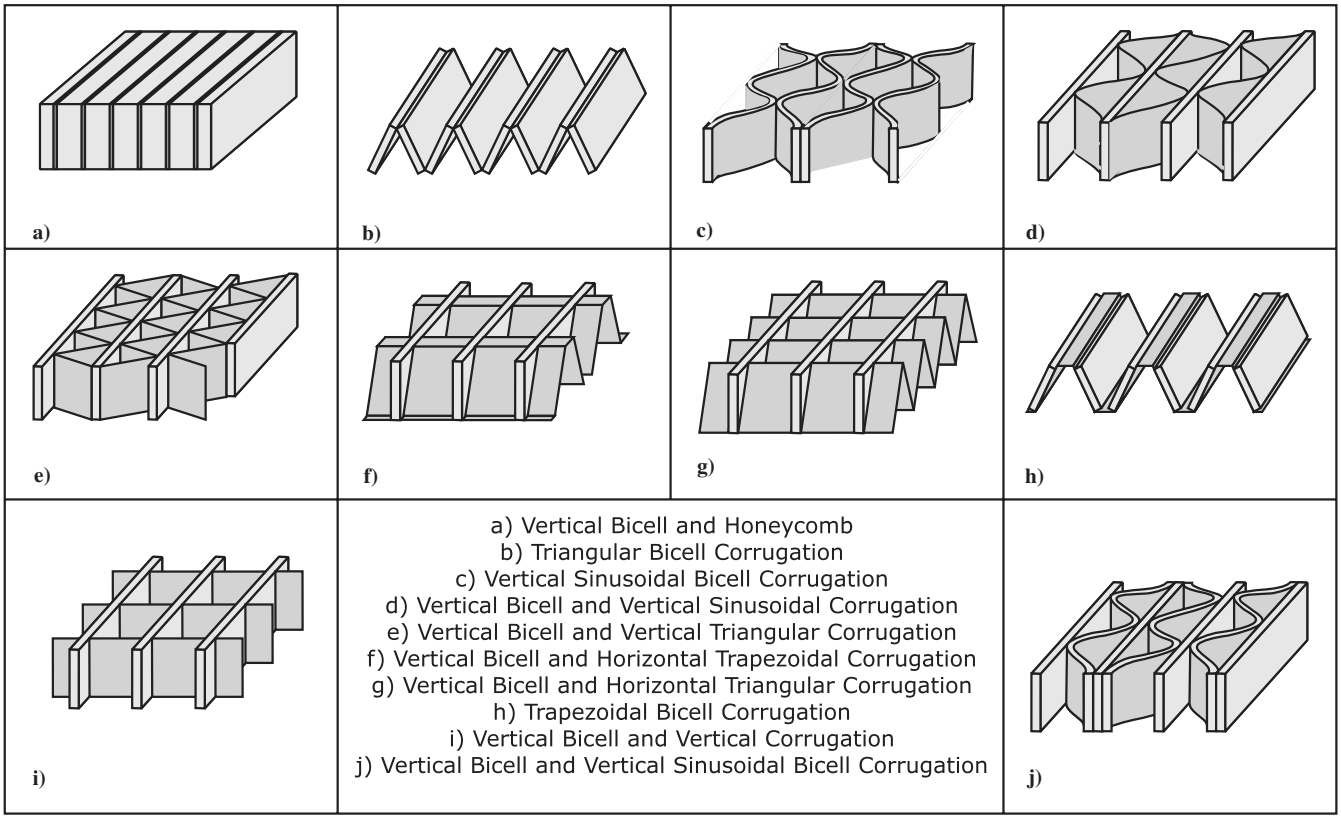

Fig. 1 Ten investigated designs with flat and sinusoidal batteries.

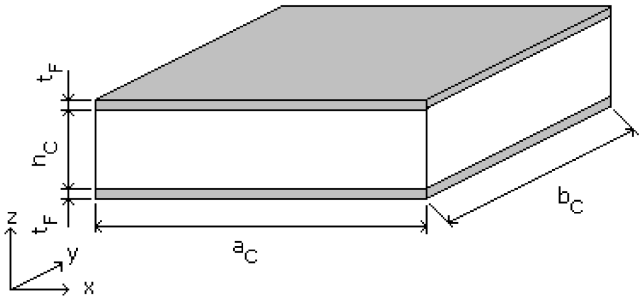

Fig. 2 The geometrical parameters used by Raville's [17] model.

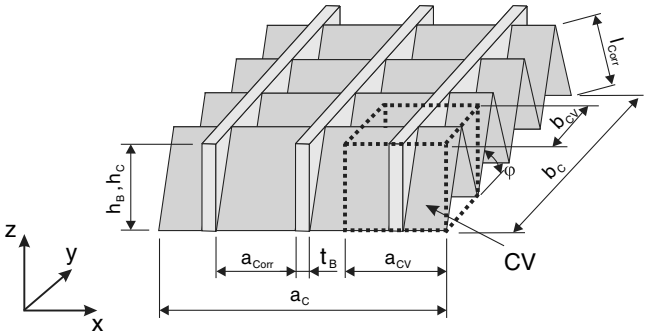

Fig. 3 Vertical bicell and horizontal triangular corrugation design.

derived. A minimization of the total energy of the system, incorporating the boundary conditions introduced by Hoff [19], leads to an expression for the natural frequency ω_P with the face sheet thickness t_F, Young's modulus E_F, density ρ_F, and Poisson's ratio ν_F

$$\omega_P^2 = \frac{E_F(\xi^2+\eta^2)^2}{\rho_F(1-\nu_F^2)h_C^4}\left(I_F + \frac{I_T}{1+S_{ij}}\right) \tag{1}$$

with

$$I_F = \frac{t_F^3}{6}, \qquad I_T = \frac{t_F}{2}(h_C+t_F)^2 \qquad W = \frac{h_C t_F}{2}\frac{\pi^2}{b_C^2}\frac{E_F}{G_{C_{xz}}(1-\nu_F^2)}$$

$$S_{ij} = \frac{W}{\Lambda_{ij}}\left(\frac{(i^2+j^2\delta^2)^2}{\delta^2} + \frac{i^2 j^2 r(1-1/r)^2}{1+\Lambda_{ij}(W/\delta^2)[(1-\nu_F)/2]r}\right)$$

$$r = \frac{G_{C_{xz}}}{G_{C_{yz}}}, \qquad \Lambda_{ij} = i^2 + \frac{j^2\delta^2}{r}, \qquad \delta = \frac{a_C}{b_C}, \qquad \xi = \frac{i\pi h_C}{a_C}$$

$$\eta = \frac{j\pi h_C}{b_C}$$

The mode numbers along length and width of the panel, i and j, are set to $i = j = 1$ in the current analysis for the required first natural frequency (fundamental "breathing" mode).

The assumption of an infinite Young's modulus E_{C_z} leaves two unknown equivalent core material properties for consideration, the out-of-plane shear moduli $G_{C_{xz}}$ and $G_{C_{yz}}$ which have a significant influence on the dynamic response of the panel [20]. Previous approaches to obtain the major out-of-plane equivalent material properties of an orthotropic core focused on particular core geometries with uniform core materials [21–25], or used simple designs for comparative studies [26]. These theories must be adapted and expanded for the equivalent shear moduli of the multifunctional designs considered in this study to accommodate the multidirectional complex layouts based on different materials.

A common approach to determine the orthotropic material properties of honeycomb and corrugated cores is the virtual displacement method: "For a virtual displacement of a system from its equilibrium position the total work performed by the internal and external forces must equal zero" [27]. To determine the equivalent out-of-plane shear moduli of the multifunctional cores, the bending, shear, and axial strain energies of the MFS caused by a virtual displacement must be equal to the strain energy of the equivalent core material subjected to the same virtual displacement. This approach enables the simple and flexible modeling of the different MFS designs and allows an effective comparison of the equivalent core material properties. Several assumptions and simplifications have been made for the analysis of the multifunctional power structures:

1) the material behaves linear-elastically [25];

2) perfect bonding exists at the face to core contacts and the rotational stiffness introduced by Wiernicki et al. [28] is neglected;

3) the joint between the bicells and additional core materials has been neglected to simplify the mathematical model as it does not significantly influence the shear stiffness;

4) the face sheets are perfectly rigid as the in-plane stiffness is an order of magnitude higher than the shear stiffness of the core;

5) the influence of the unrestrained edges is neglected and pure shear is assumed;

6) the geometry of the bicell and the corrugation allows the use of slender beam theory for bending deformation analysis.

The evaluation of the out-of-plane shear moduli $G_{C_{xz}}$ and $G_{C_{yz}}$ for all ten MFS designs would go beyond the scope of this article. The analytical approach will be demonstrated in detail for the vertical bicell and horizontal triangular corrugation design shown in Fig. 3. For the other nine MFS configurations, similar methods have been applied.

The bicells are arranged perpendicular to the face sheets and are separated by triangular corrugations that are aligned parallel to the x-direction of the core, as shown in Fig. 3. The analysis of the sandwich core with length a_C, width b_C, and height h_C focuses on the smallest geometrically repeatable CV. Its width b_{CV} corresponds to one triangular corrugation with a corrugation angle φ, a corrugation length a_{CORR}, a thickness t_{CORR}, and twice the leg length l_{CORR}. The CV includes part of a bicell of length b_{CV}, height h_B, and thickness t_B, and its total length is composed of the corrugation length a_{CORR} and the bicell thickness t_B.

This control volume is used to derive the static shear moduli $G_{C_{xz}}$ and $G_{C_{yz}}$. It is regarded as an independent structure and its boundary conditions are determined by the aforementioned assumptions such as pure shear and bending of the components and perfectly rigid face sheets.

A. Shear Modulus $G_{C_{xz}}$ of the Vertical Bicell and Horizontal Triangular Corrugation Design

By neglecting the shear deformation of the bicell during bending, the total strain energy of the remaining slender beam can be expressed as the axial and bending strain energy of a beam $U_{B_{xz}}$

$$U_{B_{xz}} = \frac{1}{2}\int_0^{h_B}\left(\frac{N_I^2}{E_{B_z}t_B b_{\mathrm{CV}}} + \frac{M_I^2}{E_{B_z}J_{B_y}}\right)\mathrm{d}s_I \tag{2}$$

With reference to Fig. 4a, the equilibriums of forces and moments for the bicell can be defined

$$\sum F_x\colon H_{AA} - F_B = 0 \qquad \sum F_z\colon V_{AA} - V_{CC} = 0$$
$$\sum M_{AA}\colon M_{AA} + M_{CC} + F_B h_B = 0 \tag{3}$$

The bending moments M and the axial forces N of the beam become

$$M_I = -M_{AA} - H_{AA}s_I \qquad N_I = -V_{AA} \tag{4}$$

To solve the two times statically indeterminate system, Castigliano's [29] and Menabrea's [30] theorems are used, respectively. Building on the displacement method, Castigliano states, "For a linear structure the partial derivation of the strain energy with respect to any load F is equal to the corresponding displacement u provided that the strain energy is expressed as a function of the loads." The displacement u_B of the bicell caused by the force F_B becomes

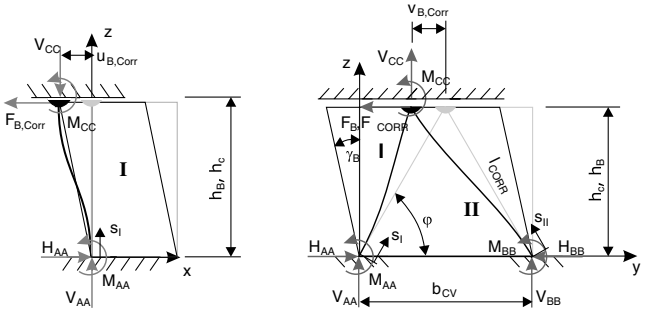

a) x–z plane **b) y–z plane**

Fig. 4 Shear deformation in the *x–z* and *y–z* plane.

$$u_B = \frac{\partial U_{B_{xz}}}{\partial F_B} \tag{5}$$

Extending Castigliano's theorem, Menabrea's principle differentiates Eq. (5) for the unknown reaction force whose work-displacement is zero, providing a further two equations

$$\left.\begin{array}{l} \frac{\partial U_{B_{xz}}}{\partial M_{AA}} = 0 \\ \frac{\partial U_{B_{xz}}}{\partial V_{CC}} = 0 \end{array}\right\} \Rightarrow M_{AA}, V_{CC} \tag{6}$$

and transforming the system to a statically determined state. The strain energy of the deformed bicell can now be expressed in terms of the deforming force F_B with the second area moment of inertia of the bicell $J_{B_y} = 1/12 t_B^3 b_{\mathrm{CV}}$

$$U_{B_{xz}} = \frac{1}{24}\frac{F_B^2 h_C^3}{E_{B_z} J_{B_y}} \tag{7}$$

The two legs of corrugation included in the control volume undergo simple shear. The general strain energy for an elastic body can be expressed in terms of stress and strain [27]

$$U = \frac{1}{2}\int_V (\sigma_x \epsilon_x + \sigma_y \epsilon_y + \sigma_z \epsilon_z + \tau_{xy}\gamma_{xy} + \tau_{yz}\gamma_{yz} + \tau_{xz}\gamma_{xz})\,\mathrm{d}V \tag{8}$$

which leads to the shear strain energy of the corrugation

$$U_{\mathrm{CORR}_{xz}} = \frac{1}{4}\frac{F_{\mathrm{CORR}}^2 l_{\mathrm{CORR}}}{G_{\mathrm{CORR}_{xz}} a_{\mathrm{CORR}} t_{\mathrm{CORR}}} \tag{9}$$

and similarly for the entire control volume to

$$U_{\mathrm{CV}_{xz}} = \frac{1}{2}\frac{F_{\mathrm{CV}}^2 h_C}{G_{\mathrm{CV}_{xz}} a_{\mathrm{CV}} b_{\mathrm{CV}}} \tag{10}$$

Using the equilibrium of forces $F_{\mathrm{CV}} = F_B + F_{\mathrm{CORR}}$ and evaluating the equilibrium of the potential energies $U_{\mathrm{CV}_{xz}} = U_{B_{xz}} + U_{\mathrm{CORR}_{xz}}$ leads to the equivalent shear modulus $G_{\mathrm{CV}_{xz}}$ of the vertical bicell and horizontal triangular corrugation design

$$G_{C_{xz}} = 2\frac{h_C\left(h_B^3 G_{\mathrm{CORR}_{xz}} a_{\mathrm{CORR}} t_{\mathrm{CORR}} + \frac{1}{2} l_{\mathrm{CORR}} E_{B_z} t_B^3 b_{\mathrm{CV}}\right)}{h_B^3 a_{\mathrm{CV}} b_{\mathrm{CV}} l_{\mathrm{CORR}}} \tag{11}$$

B. Shear Modulus $G_{C_{yz}}$ of the Vertical Bicell and Horizontal Triangular Corrugation Design

The strain energy of the control volume in the *y–z* plane is composed of the shear deformation of the bicell and the bending of the corrugation (see Fig. 4b). The equilibrium of forces and moments for the two corrugation legs can be expressed as

$$\begin{gathered} \sum F_x\colon H_{AA} - H_{BB} - F_{\mathrm{CORR}} = 0 \\ \sum F_z\colon V_{AA} + V_{BB} + V_{CC} = 0 \\ \sum M_{AA}\colon M_{AA} + M_{BB} + M_{CC} + 2l_{\mathrm{CORR}}\cos\varphi V_{BB} \\ + V_{CC} l_{\mathrm{CORR}}\cos\varphi + F_{\mathrm{CORR}} l_{\mathrm{CORR}}\sin\varphi = 0 \end{gathered} \tag{12}$$

and the bending moments and the axial forces of the two beams become

$$\begin{aligned} M_I &= V_{AA} s_I \cos\varphi - H_{AA} s_I \sin\varphi - M_{AA} \\ N_I &= -V_{AA}\sin\varphi - H_{AA}\cos\varphi \\ M_{II} &= -V_{BB} s_{II}\cos\varphi + H_{BB} s_{II}\sin\varphi - M_{BB} \\ N_{II} &= -V_{BB}\sin\varphi - H_{BB}\cos\varphi \end{aligned} \tag{13}$$

Applying Castigliano's and Menabrea's theorems gives an expression for the potential energy stored in the corrugation legs. The bicell experiences simple shear in the *y–z* direction and from the equilibrium of the potential energies the equivalent shear modulus $G_{C_{yz}}$ of the vertical bicell and horizontal triangular corrugation design can be calculated

$$\begin{aligned} G_{C_{yz}}^{up} &= \frac{h_C(XX + YY + ZZ)}{l_{\mathrm{CORR}}^3 a_{\mathrm{CV}} b_{\mathrm{CV}} h_B} \\ XX &= 2h_B t_{\mathrm{CORR}} a_{\mathrm{CORR}} E_{\mathrm{CORR}_z} l_{\mathrm{CORR}}^2 \cos^2\varphi \\ YY &= 2t_{\mathrm{CORR}}^3 a_{\mathrm{CORR}} E_{\mathrm{CORR}_z} h_B (1 - \cos^2\varphi) \\ ZZ &= G_{B_{yz}} t_B b_{\mathrm{CV}} l_{\mathrm{CORR}}^3 \end{aligned} \tag{14}$$

Similar approaches were used to calculate the two equivalent out-of-plane shear moduli for the nine other proposed MFS designs (not reported here).

The accuracy of the derived analytical expressions for the equivalent out-of-plane shear moduli $G_{C_{xz}}$ and $G_{C_{yz}}$ was investigated by corresponding simplified three-dimensional finite element (FE) models. Each control volume was modeled in Ansys 7.1 using SHELL63 elements for the bicells and the corrugation and SOLID73 elements for the honeycomb core. The finite element models were subjected to the simplifications of the analytical approaches, including a forced simple shear in the bicells and the corrugation, perfect bonding between the facings and the core and no bonding between the different core components to provide comparable results. A unit force was applied to the models and from their predicted displacement the equivalent shear moduli of the FE models were calculated.

IV. Parameter Optimization of MFS Sandwich Panels

The application of the multifunctional power structure has three major objectives:

1) high stiffness to comply with launch authority requirements and to ensure structural integrity during launch;

2) a low material density for a lightweight spacecraft;

3) a high power density to provide the necessary energy.

A parameter optimization was carried out for the ten candidate multifunctional structures presented in Fig. 1, to determine the most promising design.

To find the optimal balance between the highest first natural frequency ω_P [see Eq. (1)] and the lowest material density $\rho_{P_{\mathrm{mat}}}$ of the panels the frequency-density ratio Γ is introduced which condenses the structural behavior of the MFS into a single value and becomes the major parameter for the optimization

$$\Gamma = \frac{\omega_P}{\rho_{P_{\mathrm{mat}}}} \tag{15}$$

Raville's [17] frequency equation [Eq. (1)] emphasizes the strong impact of the face sheet material properties E_F, ρ_F, and ν_F, the thickness of the facings t_F, the two out-of-plane shear moduli of the core $G_{C_{xz}}$ and $G_{C_{yz}}$, and the core thickness h_C on the dynamic response of the simple supported sandwich panel. The use of aluminum for the facings and the corrugation eliminates several unknowns from the frequency equation and reduces the variables to the face skin thickness t_F, the core thickness h_C, and the main out-of-plane core shear moduli $G_{C_{xz}}$ and $G_{C_{yz}}$. These four parameters were modified during the parameter optimization of the frequency-density ratio to ensure a MFS core configuration with a high shear stiffness and a low density.

The core shear moduli depend strongly on the design of the different MFS introducing core geometry values into the optimization. Some of these new parameters are directly related to the overall panel dimensions and the required number of bicells, and are not available for the optimization. Others such as the number of corrugations n_{CORR} and their thickness t_{CORR} become valuable optimization inputs. They may be restricted by upper and lower limits to ensure compliance with manufacturing and flight specifications, and to minimize localized effects in the panels. The optimization was carried out in MATLAB 6.5 with the implemented optimization toolbox (version 2.2) which enabled the minimization and maximization of several functions with multiple parameters within set boundaries and permitted additional constraints.

Detailed three-dimensional finite element models were created with the dimensions of the analytically optimized sandwich panels to compare and validate the results and investigate additional issues such as local resonances of the face skin or the corrugation. The models were created in Ansys 7.1 using SHELL63 and SOLID45 elements with perfect bonding between all components and a simple support along the four edges. In addition, the material properties provided by the analytical optimization were applied to an equivalent FE model of a sandwich panel to get a further indication of the accuracy of the analytical approach. This model consisted of three layered SHELL91 elements with an activated sandwich option and had a simple support along the four edges.

To compare the dynamic behavior of the ten optimized MFS panels, a conventional honeycomb core sandwich panel was included in the analysis. This provided a comparison between frequency-density ratio values for the analytical and the finite element approaches.

V. Results and Discussion

The investigation into the dynamic behavior of multifunctional power structures yielded two main results: the equivalent out-of-plane shear moduli $G_{C_{xz}}$ and $G_{C_{yz}}$ of the different core designs, and the optimized dynamic response of the panels.

A. Simplified Material Properties

The equivalent shear moduli of the ten investigated designs provided by the simplified analytical method were calculated for a single geometry and compared with the results of the finite element analysis for a better understanding of their accuracy. Identical dimensions and material properties, which did not yet represent optimized values, were used for both methods.

The analytical and finite element values for the shear moduli of the different core designs are listed in Table 1 along with their percentage difference. The two methods were in good agreement for most designs with less than 0.5% variation between the analytical and finite element results. An exception in the x–z plane was the trapezoidal bicell corrugation design where the analytical model of this particular design assumed combined material properties of the corrugation and the core in a single sheet, whereas the finite element analysis used a double layered shell element with a separated corrugation and bicell layer. The variation in the results of the sinusoidal bicell corrugations design in the y–z plane were due to effects such as local deformations in the finite element analysis which were neglected in the analytical method.

The preliminary equivalent shear moduli $G_{C_{xz}}$ and $G_{C_{yz}}$ of the cores were already in the range of conventional honeycomb cores. Despite several simplifications in the analytical models, their results were in a good agreement with the FE analysis and provided a reliable input for the following parameter optimization.

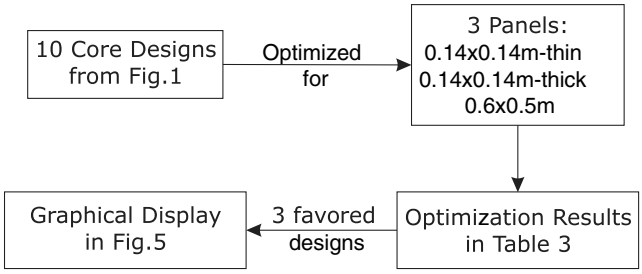

Fig. 5 Optimization process.

B. Analytical Parameter Optimization of the MFS

An analytical parameter optimization was carried out to calculate and improve the dynamic behavior of the ten MFS core designs from Fig. 1. These designs were optimized for three different sandwich panel sizes, described later herein. From the obtained results, the three best configurations were chosen for each panel size, and considered in greater detail. This optimization process is illustrated in Fig. 5.

Two of the sandwich panels investigated were $0.14 \times 0.14 \times 0.02$ m in size, based on the estimated battery dimensions. The face skin thickness t_F and corrugation thickness t_{CORR} were constrained between two boundaries with a thinner sheet size limit for the first configuration (0.14×0.14 m-thin) and a thicker one for the second (0.14×0.14 m-thick) to minimize local buckling and resonances. A third 0.6×0.5 m-sized sandwich panel was based on a flexible bicell size with a variable core height h_C. All input values for the parameter optimization are listed in Table 2. Most variables converged towards the set lower limits during the optimization of the frequency-density ratio, leading to thinner wall thicknesses and fewer corrugations with a strong decrease in the density.

Table 1 Equivalent shear moduli $G_{C_{xz}}$ and $G_{C_{yz}}$ of the analytical and finite element method

Design	$G_{C_{xz}}$, MPa Analytical	FE	%	$G_{C_{yz}}$, MPa Analytical	FE	%
a) Vertical bicell and honeycomb	406	406	0.00%	458	458	0.00%
b) Triangular bicell corrugation	264	264	−0.12%	390	390	0.02%
c) Vertical sinusoidal bicell corrugation	596	593	−0.51%	119	122	2.43%
d) Vertical bicell and vertical sinusoidal corrugation	630	628	−0.20%	395	395	− 0.03%
e) Vertical bicell and vertical triangular corrugation	634	631	−0.46%	378	378	0.14%
f) Vertical bicell and horizontal trapezoidal corrugation	389	389	0.00%	388	389	0.14%
g) Vertical bicell and horizontal triangular corrugation	508	507	−0.23%	473	475	0.51%
h) Trapezoidal bicell corrugation	315	307	−2.62%	773	774	0.18%
i) Vertical bicell and vertical corrugation	348	348	0.11%	257	257	0.00%
j) Vertical bicell and vertical sinusoidal bicell corrugation	542	539	−0.55%	383	386	0.75%

Table 2 Input parameters of the optimization

Bicell	0.14 × 0.14-thin	0.14 × 0.14-thick	0.6 × 0.5
n_B	4|→20	4|→20	10|→50
t_B	0.0015	0.0015	0.0015
h_B, m	0.02	0.02	0.01|→0.05
a_C, m	0.14	0.14	0.6
b_C, m	0.14	0.14	0.5
E_{B_z}, MPa	8000	800	800
$G_{B_{yz}}$, MPa	3000	300	300
ρ_B, kg/m^3	1550	1550	1550
power$_B$, Ah	0.25	0.25	0.25
Facing			
E_F, MPa	70,000	70,000	70,000
ν_F	0.33	0.33	0.33
ρ_F, kg/m^3	2700	2700	2700
t_F, m	0.0005– 0.003	0.001–0.003	0.001–0.003
MFS honeycomb			
type	3.4-1/4-15 (3003)	3.4-1/4-15 (3003)	1.8-3.4-25 (5052)
E_F, MPa	540	540	165
$G_{H_{xz}}$, MPa	130	130	96
$G_{H_{yz}}$, MPa	260	260	182
ρ_H, kg/m^3	45	45	29
Corrugation			
n_{CORR}	2|→8	2|→8	4|→28
E_{CORR_z}, MPa	70,000	70,000	70,000
ν_{CORR}	0.33	0.33	0.33
$G_{\mathrm{CORR}_{xz}}$, MPa	26,300	26,300	26,300
ρ_{CORR}	2700	2700	2700
t_{CORR}, m	0.0004–0.0014	0.0005–0.0014	0.0005–0.002
$c_{\mathrm{CORR}_{\min}}$, m	0.005–0.02	0.005–0.02	0.005–0.04
Honeycomb comparison panel			
type	3.4-1/4-15 (3003)	5.2-1/4-25 (3003)	——
E_F, MPa	540	1000	——
$G_{H_{xz}}$, MPa	130	220	——
$G_{H_{yz}}$, MPa	260	440	——
ρ_H, kg/m^3	45	83	——

The parameter optimization of the three sandwich panels provided five "performance" indices for each of the ten core designs on which a final decision could be based (see Fig. 6). A high frequency-density ratio was the most important parameter to provide a space qualified structure, followed by a high first natural frequency ω_P of the panels and a low material density $\rho_{P_{\mathrm{mat}}}$. A high power density $\rho_{P_{\mathrm{pow}}}$ and a balanced isotropic behavior of the panels were not the main focus of the dynamic optimization and had a lesser influence on the final design decision. The values presented for the two 0.14×0.14 m panels were based on seven bicells, used by Boundless for their demonstration panel,[§] and 20 bicells for the larger panel with a similar $\rho_{P_{\mathrm{pow}}}$. Based on the results from Fig. 6, the three most promising core designs for each sandwich panel were chosen for a more detailed discussion: the vertical bicell and honeycomb, the vertical bicell and horizontal triangular corrugation, and the vertical bicell and vertical corrugation designs.

The most important result was the frequency-density ratio Γ which is indicative of the overall performance of the panels. The 0.14×0.14 m-thin and the 0.6×0.5 m panels provided the highest Γ values for the vertical bicell and vertical corrugation design, with slightly smaller values for the other two designs. The 0.14×0.14 m-thick panels provided a clearer distinction, with the vertical bicell and horizontal triangular corrugation design exceeding the other two Γ values by more than 7%. A successful application of the MFS in a spacecraft required a high first natural frequency. The vertical bicell and horizontal triangular corrugation design gave the highest frequency values for all three panels and the other two designs provided up to 30% lower values. An advantage of the two latter designs was their lower material density $\rho_{P_{\mathrm{mat}}}$, which reduces the launch costs of a spacecraft. The power density $\rho_{P_{\mathrm{pow}}}$, as the main electrical systems parameter, was highest for the lighter designs where a fixed number of bicells linked it directly to the material densities. The isotropy values in Fig. 6 showed the percentage deviation of the out-of-plane shear modulus $G_{C_{xz}}$ from $G_{C_{yz}}$ with 100% representing equal material properties. Large variations could be found in this category with the vertical bicell and horizontal triangular corrugation design providing the closest isotropic behavior for the 0.14×0.14 m-thin and the 0.6×0.5 m panels, and the vertical bicell and vertical corrugation design for the 0.14×0.14 m-thick panel.

The vertical bicell and vertical corrugation design resulted in slightly higher Γ values for the 0.14×0.14 m-thin and the 0.6×0.5 m sandwich panels, and the vertical bicell and horizontal triangular corrugation design provided the better result for the 0.14×0.14 m-thick panel. The latter design also provided higher first natural frequencies for all of the investigated panel sizes and became the favored design for satellite multifunctional power structures.

C. Finite Element Analysis of the MFS panels

The analytical results were compared with the detailed and equivalent three-dimensional finite element models of the panels to evaluate the influence of the assumed simplifications and investigate the effects of local instabilities in the facings and corrugation. Software restraints on the maximum allowed number of nodes limited the detailed FE analysis to the two 0.14×0.14 m panels and prevented an FE analysis of the 0.6×0.5 m structure. The finite element frequency-density ratios were derived from the first natural frequencies of the modal analysis and the total element mass of the FE models.

The analytical and finite element values of the frequency-density ratios and the first natural frequencies for the three candidate designs

[§]Data available on-line at http://www.boundlesscorp.com/EnergyStorage.htm [cited 27 June 2005].

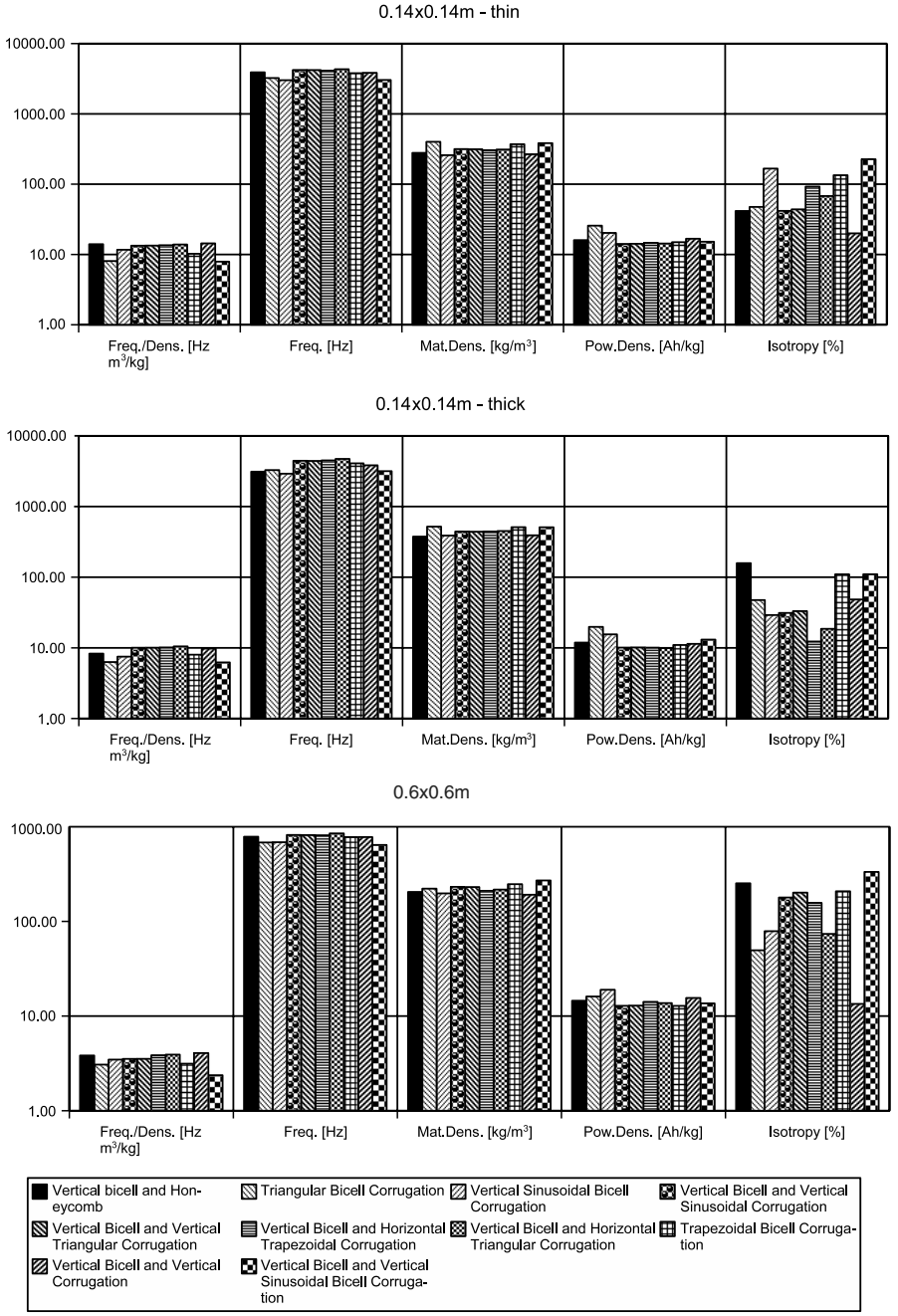

Fig. 6 Results of the analytical optimization for the ten MFS panels.

from the optimization are presented in Figs. 7 and 8, along with the values of a conventional honeycomb panel. The highest frequency-density ratios were provided in all but one case by the simplified analytical optimization. This was due to a series of assumptions for the calculation of the out-of-plane core shear moduli: simplifications introduced in Raville's [17] model, and a set of local effects such as deformations in the facings and the core detected by the finite element models.

The equivalent FE models, using the out-of-plane core shear moduli from the optimization, showed 5–7% lower Γ values than the

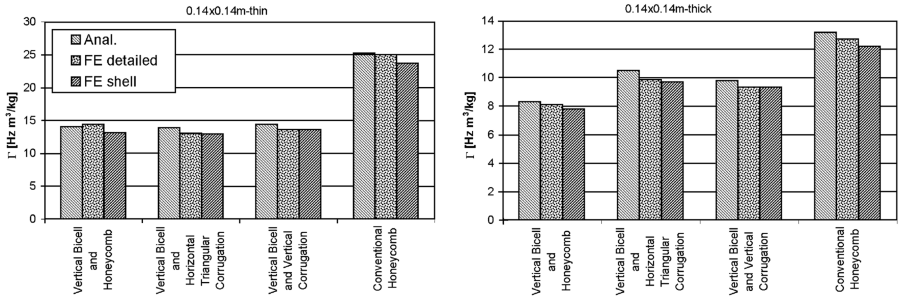

Fig. 7 Analytical and FE results for the frequency-density ratio of three candidate designs.

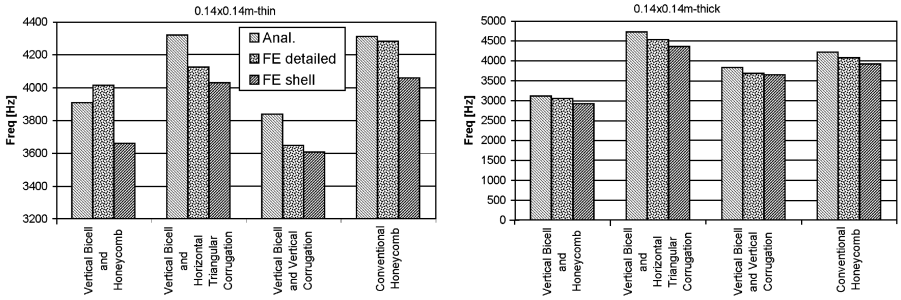

Fig. 8 Analytical and FE results for the first natural frequency of three candidate designs.

Fig. 9 Vertical bicell and horizontal triangular corrugation test panel.

analytical methods. This highlighted the influence of Raville's assumptions on the dynamic behavior, particularly as no infinite out-of-plane Young's modulus E_{C_z} could be applied to the equivalent finite element material properties. The optimization and the equivalent FE model of the 0.14×0.14 m-thin sandwich panels produced the highest Γ values for the vertical bicell and vertical corrugation design, whereas the detailed FE analysis predicted the highest values for the vertical bicell and honeycomb design. This inconsistency could be ascribed to the solid elements used for the honeycomb core that provided a perfect support for the thin face skins and prevented any local deformation. Optimization, detailed FE, and equivalent FE of the 0.14×0.14 m-thick panel calculated the highest Γ values for the vertical bicell and horizontal triangular corrugation design.

All of the first natural frequency values Fig. 8 showed a clear preference for the vertical bicell and horizontal triangular corrugation design, which provided the highest values in all investigated cases. The vertical bicell and vertical corrugation design had up to 20% lower frequency values with the high frequency-density ratios $\Gamma = \omega_P / \rho_{P_{\text{mat}}}$ ascribed solely to the lower density of the design.

The conventional honeycomb panels had higher frequency-density ratios because of their lower density, but the vertical bicell and horizontal triangular corrugation design achieved similar or even better first natural frequency values. The optimized geometries of the MFS designs effectively counterbalanced the disadvantage of the additional weight by providing a stiffer core structure.

The three candidate designs resulted in a comparable performance of the frequency-density ratios during the optimization and FE analysis, and no clear favorite could be identified. The first natural frequencies of the panels allowed a better distinction. The frequencies of the vertical bicell and horizontal triangular corrugation significantly exceeded the vertical bicell and vertical corrugation values in all examined configurations and became the chosen design for future space application. The comparable dynamic behavior of the vertical bicell and horizontal triangular corrugation to ordinary honeycomb core sandwich panels, and the overall weight and volume reduction of a spacecraft offered by a multifunctional power approach, made it an optimum choice for future low weight space missions.

This study went on to use experimental data to validate the presented theoretical results. A vertical bicell and horizontal triangular corrugation panel has been manufactured (see Fig. 9) and its dynamic behavior tested. Initial results have shown good agreement with the theoretical values. A detailed discussion of these results is outside the scope of this paper, and will be presented in a future publication.

VI. Conclusions

Ten possible designs for a multifunctional power structure for space applications have been presented and their dynamic behavior was analyzed and optimized. A simplified analytical model for the required out-of-plane core shear moduli was derived and has been validated against FE models of the structure. A parameter optimization of the MFS panels was carried out and their dynamic response was compared with detailed and equivalent three-dimensional finite element models. A good agreement between the different approaches was found and two particular designs with vertical bicell orientation and simple or triangular aluminum corrugation emerged as the best options for a multifunctional space structure. It was shown that the chosen multifunctional design with its integrated power storage system provided a similar dynamic behavior compared with a conventional structural honeycomb core sandwich panel, which makes an MFS approach an excellent choice for future low cost space missions.

References

[1] Haake, J. M., Jacobs, J. H., and McIlroy, B. E., "Thick Walled Carbon Composite Multifunctional Structures," *Proceedings of SPIE: International Society for Optical Engineering*, Vol. 3041, March 1997, pp. 32–43.

[2] Rossoni, P., and Panetta, P. V., "Developments in Nano-Satellite Structural Subsystem Design at NASA-GSFC," AIAA Paper TS-V-3, 1999.

[3] Fosness, E., Guerrero, J., Qassim, K., and Denoyer, S. J., "Recent Advances in Multi-Functional Structures," *Proceedings of the 2000 Institute of Electrical and Electronic Engineers (IEEE) Aerospace Conference*, Vol. 4, Institute of Electrical and Electronics Engineers, New York, March 2000, pp. 23–28.

[4] Guerrero, J., Fosness, E., and Buckley, S., "Multifunctional Structures," *Proceedings of AIAA Space 2001*, AIAA Paper 2001-4585, 2001.

[5] Hill, C. A., "Satellite Battery Technology: A Tutorial and Overview," *Proceedings of 1998 Institute of Electrical and Electronic Engineers (IEEE) Aerospace Conference*, Vol. 1, Institute of Electrical and Electronics Engineers, New York, March 1998, pp. 153–158.

[6] Marcelli, D., Summers, J., and Neudecker, B., "Libacore 2: Power Storage in Primary Structure," *Proceedings of 43rd AIAA Structures, Structural Dynamics, and Materials Conference*, AIAA Paper 2002-1242, 2002.

[7] Clark, C., Summers, J., and Armstrong, J., "Innovative Flexible Lightweight Thin-Film Power Generation and Storage for Space Applications," *Proceedings of 35th Intersociety Energy Conversion Engineering Conference and Exhibit (IECEC)*, AIAA Paper 2000-2922, 2000.

[8] Neudecker, B. J., Benson, M. H., and Emerson, B. K., "Power Fibers: Thin-Film Batteries on Fiber Substrates," Defense Advanced Research Projects Agency (DARPA), Synthetic Multifunctional Materials, http://www.darpa.mil/dso/thrust/matdev/smfm/present.html [cited 10 March 2005].

[9] Metzger, W., Westfall, R., Hermann, A., and Lyman, P., "Nickel Foam Substrate for Nickel Metal Hydride Electrodes and Lightweight

Honeycomb Structures," *International Journal of Hydrogen Energy*, Vol. 23, No. 11, 1998, pp. 1025–1029.
[10] Olson, J. B., Feaver, T. L., and Lyman, P. C., "Structural Lithium-Ion Batteries Using Dual-Functional Carbon Fabric Composite Anodes," Society of Manufacturing Engineers Paper TP04PUB68, July 2003.
[11] Lyman, P. C., and Feaver, T. L., "Powercore Combining Structure and Batteries for Increased Energy to Weight Ratio," *IEEE Aerospace and Electronic Systems Magazine*, Vol. 13, No. 9, 1998, pp. 39–42.
[12] Lyman, P. C., "Battery," US Patent: 5567544, 22 Oct. 1996.
[13] Lok, T. S., and Cheng, Q. H., "Free and Forced Vibration of Simply Supported, Orthotropic Sandwich Panel," *Computers and Structures*, Vol. 79, No. 3, 2001, pp. 301–312.
[14] Li, N., "Forced Vibration Analysis of the Clamped Orthotropic Rectangular Plate by the Superposition Method," *Journal of Sound and Vibration*, Vol. 158, No. 2, 1992, pp. 307–316.
[15] Gorman, D. J., "Accurate Free Vibration Analysis of Clamped Orthotropic Plates by the Method of Superposition," *Journal of Sound and Vibration*, Vol. 140, No. 3, 1990, pp. 391–411.
[16] Sakata, T., and Hosokawa, K., "Vibrations of Clamped Orthotropic Rectangular Plates," *Journal of Sound and Vibration*, Vol. 125, No. 3, 1988, pp. 429–439.
[17] Raville, M. E., and Ueng., C. E. S., "Determination of Natural Frequencies of Vibration of a Sandwich Plate," *Experimental Mechanics*, Vol. 7, No. 11, 1967, pp. 490–493.
[18] Narayana, K. B., Ramanath, K. S., and Bonde, D. H., "Modeling Honeycomb Sandwich Panels with Shell Elements in Finite Element Analysis," *Journal of Spacecraft Technology*, Vol. 5, No. 3, 1995, pp. 33–41.
[19] Hoff, N. J., "Bending and Buckling of Rectangular Sandwich Plates," NACA TN2225, 1950.
[20] Schwingshackl, C. W., Cunningham, P. R., and Aglietti, G. S., "Honeycomb Elastic Material Properties: A Review of Some Existing Theories and a New Dynamic Approach," *Proceedings of International Conference on Noise and Vibration Engineering 2004*, Leuven, Belgium, 2004, pp. 1353–1366.
[21] Libove, C., and Hubka, E., "Elastic Constants for Corrugated-Core Sandwich Plates," NACA TN-2289, Feb. 1951.
[22] Ko, W. L., "Elastic Constants for Superplastically Formed/Diffusion-Bonded Sandwich Structures," *AIAA Journal*, Vol. 18, No. 8, 1980, pp. 986–987.
[23] Nordstrand, T. M., Carlsson, L. A., and Allen, H. G., "Transverse Shear Stiffness of Structural Core Sandwich," *Composite Structures*, Vol. 27, No. 3, 1994, pp. 317–329.
[24] Nordstrand, T. M., and Carlsson, L. A., "Evaluation of Transverse Shear Stiffness of Structural Core Sandwich Plates," *Composite Structures*, Vol. 37, No. 2, 1997, pp. 145–153.
[25] Davalos, J. F., Qiao, P., Xu, X. F., Robinson, J., and Barth, K. E., "Modeling and Characterization of Fiber-Reinforced Plastic Honeycomb Sandwich Panels for Highway Bridge Applications," *Composite Structures*, Vol. 52, Nos. 3–4, 2001, pp. 441–452.
[26] Buannic, N., Cartraud, P., and Quesnel, T., "Homogenization of Corrugated Core Sandwich Panels," *Composite Structures*, Vol. 59, No. 3, 2003, pp. 299–312.
[27] Parkus, H., *Mechanik der Festen Koerper*, 2nd ed., Springer–Verlag, New York, 1995.
[28] Wiernicki, C. J., Liem, F., Woods, G. D., and Furio, A. J., "Structural Analysis Methods for Lightweight Metallic Corrugated Core Sandwich Panels Subjected to Blast Loads," *Naval Engineers Journal*, Vol. 103, No. 3, 1991, pp. 192–203.
[29] Gere, J. M., and Timoshenko, S. P., *Mechanics of Materials*, 3rd ed., PWS Publishing, Boston, MA, 1990.
[30] Carpinteri, A., *Structural Mechanics: A Unified Approach*, 1st ed., Taylor and Francis, Philadelphia, PA, 1997.

B. Sankar
Associate Editor